Front. Chem. Sci. Eng.
https://doi.org/10.1007/s11705-018-1762-3

RESEARCH ARTICLE

Self-assembled bright luminescent hierarchical materials from a tripodal benzoate antenna and heptadentate Eu(III) and Tb(III) cyclen complexes

Aramballi J. Savyasachi[1*], David F. Caffrey[1*], Kevin Byrne[2], Gerard Tobin[2], Bruno D'Agostino[1], Wolfgang Schmitt[2], Thorfinnur Gunnlaugsson (✉)[1]

1 School of Chemistry and Trinity Biomedical Sciences Institute (TBSI), University of Dublin, Trinity College Dublin, Dublin 2, Ireland
2 School of Chemistry and Centre for Research on Adaptive Nanostructures and Nanodevices (CRANN), University of Dublin, Trinity College Dublin, Dublin 2, Ireland

Abstract The europium heptadentate coordinatively unsaturated (Eu(III)) and the terbium (Tb(III)) 1,4,7,10-tetraazacyclododecane (cyclen) complexes **1** and **2** were used in conjunction with ligand **3** (1,3,5-benzene-trisethynylbenzoate) to form the supramolecular self-assembly structures **4** and **5**; this being investigated in both the solid and the solution state. The resulting self-assemblies gave rise to metal centered emission (both in the solid and solution) upon excitation of **3**, confirming its role as a sensitizing antenna. Drop-cased examples of ligand **3**, and the solid forms of **4** and **5**, formed from both organic and mixture of organic-aqueous solutions, were analyzed using Scanning Electron Microscopy, which showed significant changes in morphology; the ligand giving rise to one dimensional structures, while both **4** and **5** formed amorphous materials that were highly dense solid networks containing nanoporous features. The surface area (216 and 119 $m^2 \cdot g^{-1}$ for **4** and **5** respectively) and the ability of these porous materials to capture and store gases such as N_2 investigated at 77 K. The self-assembly formation was also investigated in diluted solution by monitoring the various photophysical properties of **3**–**5**. This demonstrated that the most stable structures were that consisting of a single antennae **3** and three complexes of **1** or **2** (e.g., **4** and **5**) in solution. By monitoring the excited state lifetimes of the Eu(III) and Tb(III) ions in H_2O and D_2O respectively, we showed that their hydration states (the *q*-value) changed from ~2 to 0, upon formation of the assemblies, indicating that the three benzoates of **3** coordinated directly to the each of the three lanthanide centers. Finally we demonstrate that this hierarchically porous materials can be used for the sensing of organic solvents as the emission is highly depended on the solvent environment; the lanthanide emission being quenched in the presence of acetonitrile and THF, but greatly enhanced in the presence of methanol.

Keywords self-assembly, supramolecular chemistry, lanthanides, Eu(III) and Tb(III) complexes, luminescence, metallostars

1 Introduction

Hierarchical porous materials [1–4] have attracted significant interest in recent times. The use of lanthanide ions has become an important strategy for the development of luminescent self-assembly structures where the ions can be used to 'direct' the synthesis of novel and often functional supramolecular structures [5–9]. However, the development of hierarchical lanthanide based materials is where the self-assembly processes employed are relatively rare [10–15]. As many of the lanthanides possess unique photophysical properties, as well as possessing high coordination requirements, the formation of such self-assembly structures can be monitored in real time by observing the changes in the photophysical properties of the ligand or the metal ion itself in solution [16–19]. This has been particularly well explored in recent times using acyclic ligands based on di-picolinic acid derivatives and more recently other ligands such as the 2,6-bis(1,2,3-triazol-4-yl)pyridine (btp) building block [20–30]. The lanthanides are well known to form kinetically and thermodynamically stable complexes with cyclic structures

Received May 12, 2018; accepted June 28, 2018

E-mail: gunnlaut@tcd.ie

*These authors contributed equally to this work

such as 1,4,7,10-tetraazacyclododecane (cyclen) that possess three or four pendent amide or carboxylate arms giving rise to either seven or eight coordination environment around the lanthanide ion [31–39]. Such structures usually also possess either a single or two metal bound water molecules, which are labile [39], and can be exchanged for appropriate coordinating ligands, such as β-diketonates, the result being the formation of ternary complexes [40]. As coordination ligands are often aromatic, the ternary complex formation can allow for the population of the lanthanide center by sensitization of the lanthanide excited state, often referred to as the antenna affect [41]. In the case of lanthanide ions such as Eu(III) or Tb(III) this can result in the formation of 'highly' luminescent complexes. We have demonstrated that such ternary complexes self-assembly complexes of lanthanide cyclen complexes can be used as luminescent sensors for anions [41–43] or cations [44,45] as well as drugs, such as salicylic acid and phosphates [46] where the lanthanide ion emission is monitored either upon formation of the self-assembly, or upon displacement of the antenna from the ternary complex [47,48]. In addition to such self-assembly formations, lanthanide complexes have been used in the construction of so called 'metallostars' [49–55]. Here we present work on the development of an analogs systems based on the use of Eu(III) and Tb(III) cyclen based heptadentate complexes **1** and **2**, respectively. We show that upon reacting with the ligand **3** novel self-assemblies are formed where each of the lanthanide centers is coordinately saturated and form highly luminescent material, the gives rise to solid-state luminesce and can be used as nano-porous material.

2 Results and discussion

2.1 Design and synthesis

The heptadentate tri-amide cyclen lanthanide complexes **1** (Ln = Eu(III)) and **2** (Ln = Tb(III)) [56] and the ligand 1,3,5-benzene-trisethynylbenzoate **3** [57] were all synthesized in accordance with established literature procedures (Fig. 1). Ligand **3** is a π-conjugated aromatic compound, that possesses tritopic triangular topology, a feature that has previously been employed for the preparation of highly augmented MOFs using Zn(II), Cu(II) and lanthanide ions [12,58–62]. Particularly remarkable, is the rotational flexibility of the ligand along the acetylene moieties which promotes the formation of helical, interpenetrated structures [58] or MOF polymorphs using dinuclear copper (II) 'paddlewheel' secondary building units [59–61]. Similar structural effects are also observed in ligand derivatives that promote the formation of nanoscopic coordination cages [63]. Thus, the binding behavior and structural flexibility renders the selected ligand to be highly suitable for binding studies using Ln(III) containing compounds in the formation of luminescent self assembly structures. Further noteworthy are stabilizing π-π effects in metallosupramolecular systems that contain this tritopic benzoate ligand [58–61].

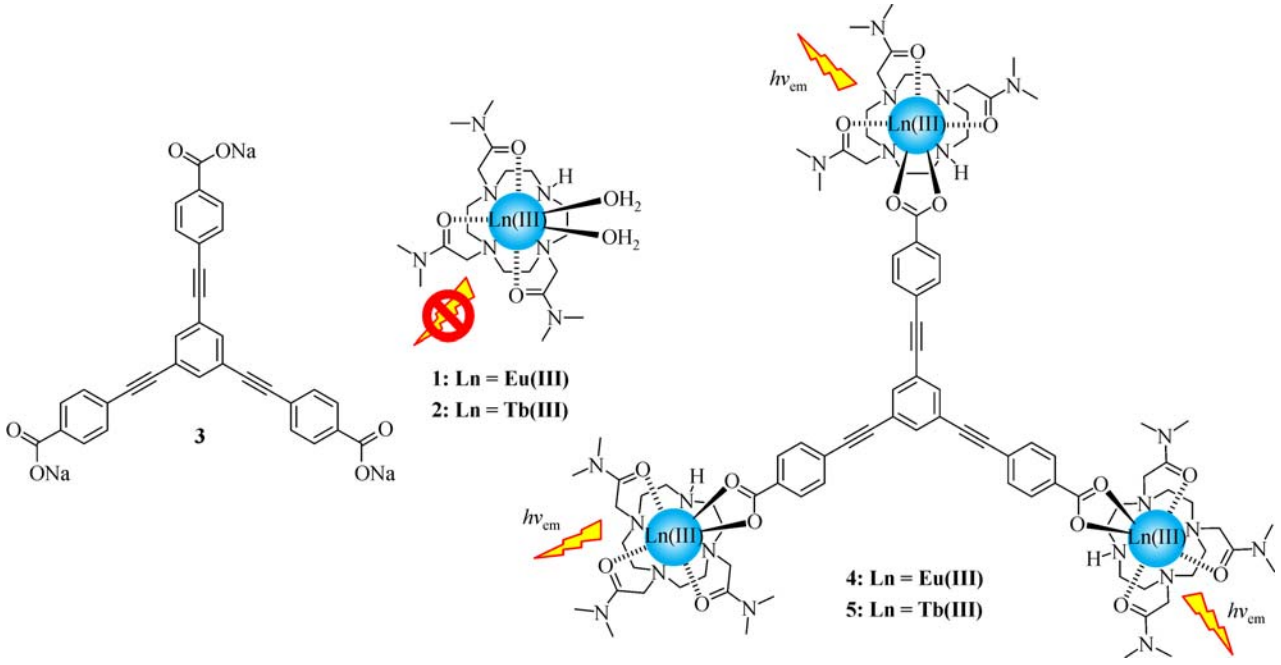

Fig. 1 The structures of the 1,3,5-benzene-trisethynylbenzoate **3**, and the cationic cyclen lanthanide complexes **1** and **2**. The displacement of the two metal bound water molecules of **1** and **2** by the antenna **3**, results in the formation of the ternary complexes, **4** and **5**. These are luminescent, giving rise to lanthanide centered emission upon excitation of the antenna which results in energy transfer to the lanthanide excited state

As discussed above, we proposed that the self-assembly between **1** or **2** and the benzoate **3** would result in the formation of 1:3 (ligand:Ln-compexes) self-assembly formation in solution, yielding **4** and **5** upon saturation. With this in mind we synthesized both **4** and **5** using microwave synthesis by simply mixing the Ln-complexes **1** and **2** with **3** in 1:3 stoichiometry in a mixture of water and CH_3CN (1:1, v:v) 90°C for 2 h. This gave on both occasions, solids upon diffusion of Et_2O into the concentrated reaction mixtures (1/3 by original vol.). However, IR spectroscopy showed that the carbonyls of **3** were shifted from 1686 to 1576 and 1576 cm^{-1}, in the case of **4** and **5** respectively, which is characteristic for the formation of such ternary complexes. The successful synthesis of these complexes was also shown by the fact that the isolated white powder was highly luminescent under UV-light activation, as well as giving rise to their respective Ln(III)-centered emission, as demonstrated in Fig. 2(b) using **4**, to a bright red emission, which is characteristic for Eu(III) when the solid state luminescent spectrum was recorded, using time gated emission (see below). Similarly, under UV-light, **5** gave rise to green emission, which is characteristic for Tb(III). The solid-state luminescence measurement performed on **4** showed the line-like emission band observed at λ = 592, 614, 651 and 700 nm, assigned to $^5D_0 \rightarrow {}^7F_J$ transitions (J = 1–4) for Eu(III), as demonstrated in Fig. 2(c) (red). In case of Tb (III) complex, Tb(III)-centered band were observed at 490, 544, 585, 616 nm, assigned to the $^5D_4 \rightarrow {}^7F_J$ transitions (J = 6–3) of Tb(III) (Fig. 2(b), green). The sensitization was further confirmed by recording the solid-state excitation spectra of Ln(III) complexes **4** and **5** upon exciting into the benzoate confirmed the successful population of their respective excited states by the antenna effect. The excited state lifetimes were also determined for these solid materials by fitting the excited state decay observed for the 615 nm ($^5D_0 \rightarrow {}^7F_2$) transition for Eu(III), and the 544 nm ($^5D_4 \rightarrow {}^7F_5$) transition of Tb(III), to a mono-exponential decay, giving τ = 0.274 ms for **4**, and τ = 0.523 ms for **5**, respectively. Giving the highly insoluble nature of the isolated material we also embarked on characterizing the morphological nature and the thermal stability of these luminescent materials were analyzed by using scanning electron microscopy (SEM) imaging.

2.2 Thermal stability and morphology studies of the ligand **3** and the Ln-self-assemblies **4** and **5**

The thermogravimetric analysis (TGA) of **4** and **5** under nitrogen atmosphere showed an initial weight loss of approximately 6% at 110°C due to the loss of solvent molecules. Further heating showed that **4** and **5** did not undergo further weight loss until they reached 390 and 420°C respectively, after which there was a weight loss of 67% in both samples indicating that they have decomposed. However, 27% of their initial weights remained beyond 600°C.

The morphology of the ligand **3** as well as of the powders formed for the self-assemblies **4** and **5** was investigated by performing SEM analysis of these systems. The ligand **3** was first analyzed and was shown to be completely soluble in both THF and in a mixture of 1:1

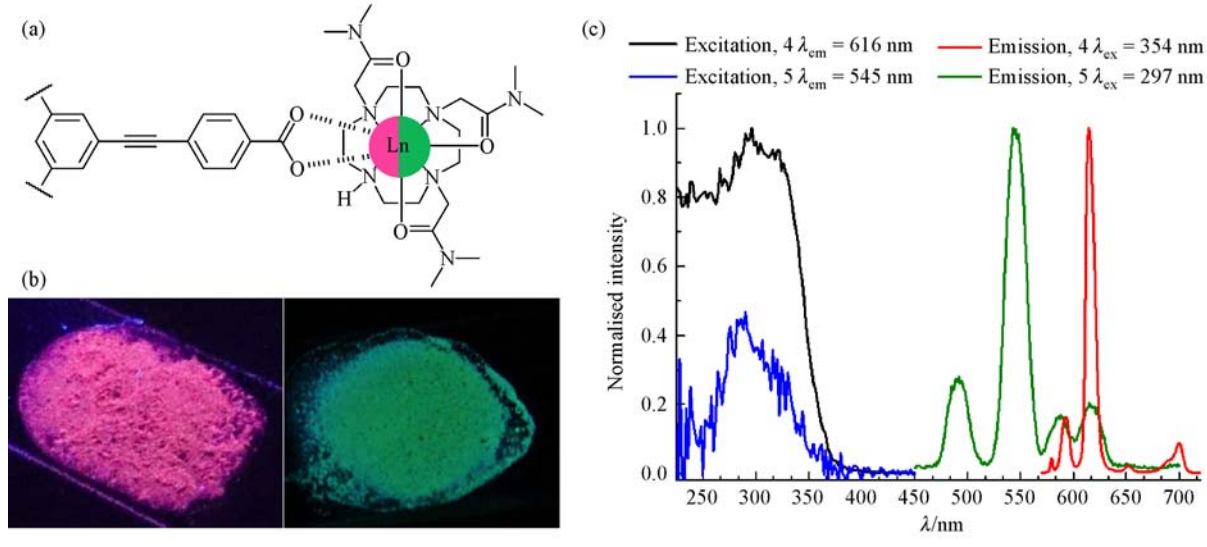

Fig. 2 (a) Diagram of the self-assembly ternary complex formation between **1** or **2** and **3** resulting in the formation of **4** and **5**; (b) the characteristic red and green luminescence seen to the naked eye upon exposing the white powder obtained of **4** and **5** to UV-light at 354 nm; (c) the characteristic Eu(III) and Tb(III) lanthanide centered emission, showing the line-line emission bands at long wavelengths, upon excitation of **4** and **5**, and the corresponding excitation spectra demonstrating that the excitation at the central tripodal antenna sensitizes the Eu(III) and the Tb(III) excited states

THF-H_2O. Compound, **3** with its central phenyl core is known to be able to self-assemble into structures consisting of helical arrangements, through π-π interactions, where the three arms are off-set; such interactions often result in the formation of one-dimensional fibers in non-competitive solvents. The SEM imaging of drop cast examples (onto silica-wafers, that were then dried in air for 12 h followed by drying in vacuum for 3 h) formed from 0.5% wt·v^{-1} solutions are shown in Fig. 3, demonstrating that indeed, **3** self-assembled in THF into entangled fibrous network. Analysis of the morphology showed that significant branching occurred, giving rise to cross-linked network of fibers, that resembled 'root-network' where the main 'roots' were of *ca*. 500 nm thickness. These were further 'cross-linked' or 'linked' into smaller networks of fibers, that were significantly thinner, with average width of *ca.* 200–300 nm. Analysis of samples of **3** that were formed from a mixture of THF-H_2O showed that in the presence of the aqueous component had significant effect on the self-assembly process and, hence, on the resulting morphology. Here, the presence of the extended cross-linked networks of fibers seen in THF was not as clearly formed, and instead, the morphology consisted of more finer and smaller areas of fibers that resembled semi-crystalline materials. This clearly demonstrating the effect the solvent alone had on the self-assembly properties of **3** and hence, the morphological outcome.

We next investigated the morphology of samples formed from **4** and **5** in both organic and organic-aqueous mixtures (in the absence of any buffer, *c.f.* later discussion on the self-assembly formation in dilute aqueous solution). Samples of (solids) of both **4** and **5** (0.5% wt·v^{-1}) were taken up into the desired solvent or solvent mixtures, and sonicated for 10 min, which gave fine suspensions that were drop-casted onto silica substrate and dried in air for 12 h followed by drying under high-vacuum for 2–3 h. All the samples were gold-coated before carrying out the SEM imaging. The results from these SEM analysis (for samples made from THF, CH_3CN and MeOH, and in 1:1 aqueous mixtures), are shown in Figs. 4 and 5, for materials **4** and **5**, respectively and clearly demonstrate that the self-assembly formation resulted in material with very different morphology to that seen above for **3**, as all the samples were found to be solid and amorphous (*c.f.* Figs. 4 and 5 for two different magnifications, for **4** and **5**, respectively). The SEM images of the dropcasted samples of **4** in THF, CH_3CN and MeOH, are shown in Figs. 4(a–c), and demonstrate the formation of hard-materials that are formed in solid blocks possessing highly porous surface. Similarly, the samples of **4** formed from aqueous mixtures 1:1 THF-H_2O, CH_3CN-H_2O and MeOH-H_2O, demonstrated the formation of larger blocks of solids that were however, broken to form smaller particles, exposing the larger area of the samples, which indicate some degree of increased porosity for those samples, as is evident from Figs. 4(d–f), most likely due to increased polarity of the solvent media. Similar observation was made for the Tb (III) complex **5**, as shown in Fig. 5. The SEM images of dropcasted solution of **5** (0.5% wt·v^{-1}) dispersed in THF, CH_3CN and MeOH showed the larger solid blocks having nano porous surface, which visually appeared to be homogenously distributed when compared to Eu(III) complex **4** (Figs. 5(a–c)). Samples of **5** prepared in aqueous mixtures of 1:1 THF-H_2O, CH_3CN-H_2O and MeOH-H_2O appeared to be more amorphous showing the homogeneously distributed fine powder (in contrast to observations made in organic solvents alone) which were formed by breaking larger particles as displayed in Figs. 5 (d–f).

The SEM images taken at higher magnifications of ~200 nm, demonstrated that the porosity of materials **4** and **5** appeared to be increased when the samples were prepared in aqueous mixtures of 1:1 THF-H_2O, CH_3CN-H_2O and MeOH-H_2O, indicating that both **4** and **5** has identical solubility behavior with minor difference in the morphological features as shown in Fig. 6. However, upon closer observation the samples of **4** showed highly nanoporous surfaces along with the presence of cavities sized approximately 100–300 nm in the solid matrix as displayed in Figs. 6(a–c). In case of **5**, 1:1 THF-H_2O sample showed porous structures with large cavities (sized 100–200 nm), and the CH_3CN-H_2O and MeOH-H_2O

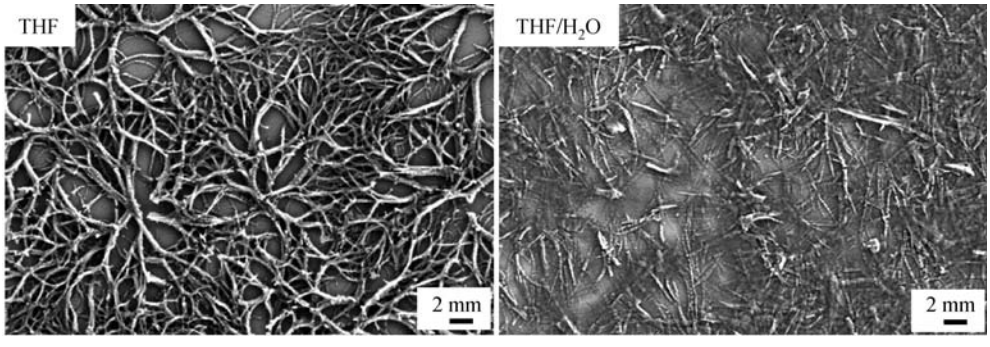

Fig. 3 The SEM images obtained from samples of 0.5% wt·v^{-1} solutions of **3** in THF (left) and 1:1 THF-H_2O (right) drop-casted onto silica wafers, scale bar 2 μm

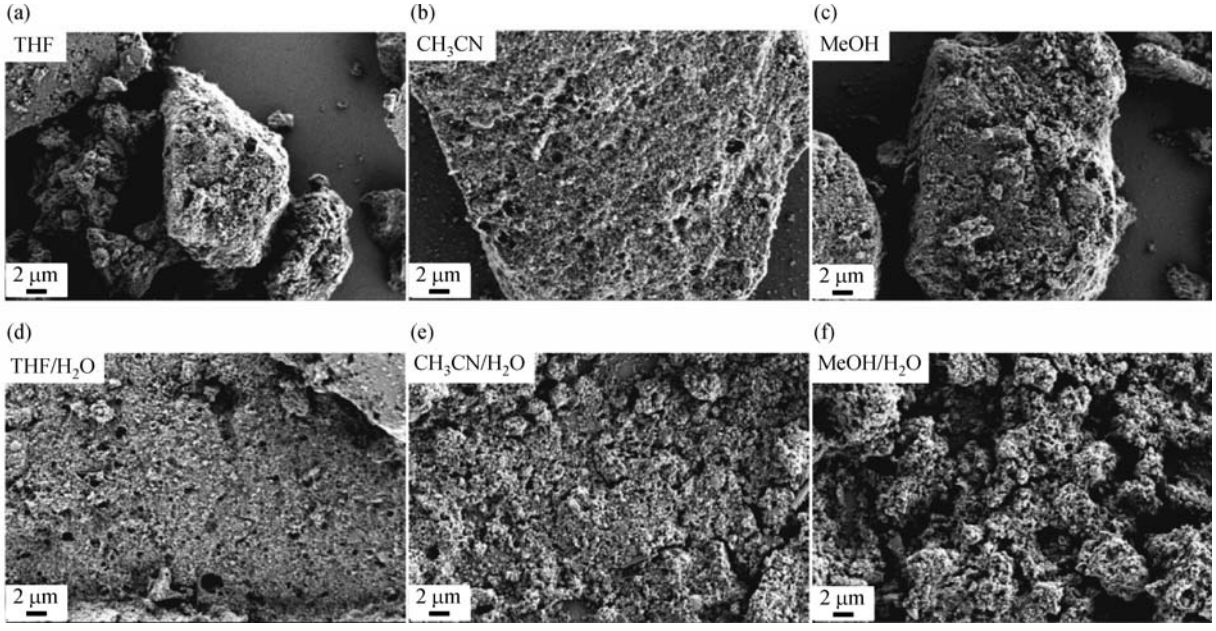

Fig. 4 SEM images of the dropcasted solutions of **4** in (a–c) THF, CH_3CN and MeOH and (d–f) the corresponding aqueous mixtures (1:1, $v \cdot v^{-1}$) THF-H_2O, CH_3CN-H_2O and MeOH-H_2O, respectively

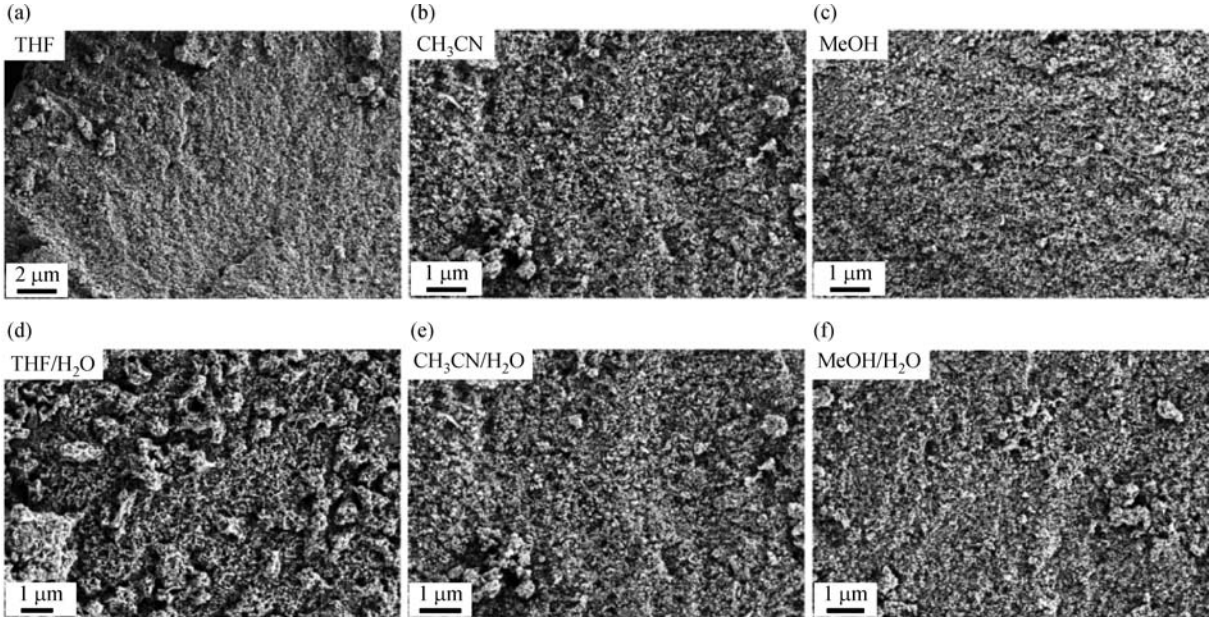

Fig. 5 SEM images of the dropcasted solutions of **5** in (a–c) THF, CH_3CN and MeOH and (d–f) the corresponding aqueous mixtures (1:1, $v \cdot v^{-1}$) THF-H_2O, CH_3CN-H_2O and MeOH-H_2O, respectively

samples showed tightly packed dense solid matrix with nanopores in contrast to the observation made in **4** as showed Fig. 6(d–f).

2.3 Gas uptake studies

Having observed the morphological features which suggest the possibility of high surface areas, these materials were tested for their gas uptake capabilities. Before the gas uptake studies were carried out, the as-synthesized powders **4** and **5** were soaked in MeCN for 48 h, refreshing the exchange solution after 24 h to remove any residual reactants and H_2O. This was followed by evacuation under dynamic vacuum at 100°C overnight

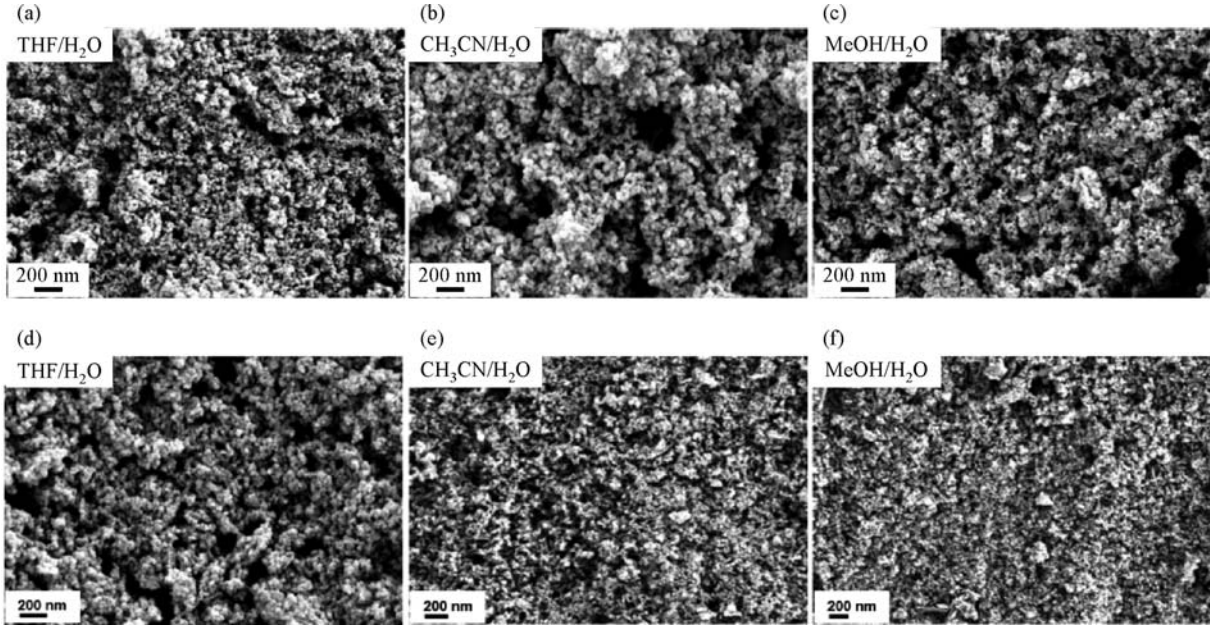

Fig. 6 SEM images taken at higher magnifications of the dropcasted solutions of (a–c) **4** and (d–f) **5** in aqueous mixtures (1:1, $v \cdot v^{-1}$) THF-H_2O, CH_3CN-H_2O and MeOH-H_2O, respectively

(taking care to avoid contact of the powders with air or moisture after activating them). For both **4** and **5**, N_2 adsorption isotherms at 77 K exhibit conventional type-II reversible adsorption-desorption isotherms and confirmed the presence of micropores in both materials. Furthermore, Density Functional Theory (DFT) pore size distributions suggest that both **4** and **5** each contain a range of micropores with diameters from 1.3 and 0.7 nm respectively (see inset in Figs. 7(a,b)). From the Brunauer-Emmett-Teller (BET) method, the surface areas were calculated to be of 216 and 119 $m^2 \cdot g^{-1}$ for **4** and **5** , respectively (Figs. 7(a,b)). The surface areas obtained from these measurements, while not as high as the best MOFs synthesized using the BTEB ligand [64]. However, they are significantly better than the measured surface area for $[Ni(Cyclam)]_3[BTEB]_2$ (6.08 $m^2 \cdot g^{-1}$) [65]. The presence of CO_2-phelic nitrogen rich Ln(III)-containing cyclen moiety inspired us to also evaluate the CO_2 and H_2 uptake properties. The CO_2 adsorption measurements at 278 K showed maximum uptakes of 46 and 64 $mg \cdot g^{-1}$ for **4** and **5**, respectively. The maximum uptakes for H_2 (at 77 K) were found to be 0.7 $mg \cdot g^{-1}$ and 3.5 $mg \cdot g^{-1}$ for **4** and **5** respectively which is low and suggests that there are very few open metal sites present in the materials.

2.4 Sensing studies

These materials were next analyzed for their sensing

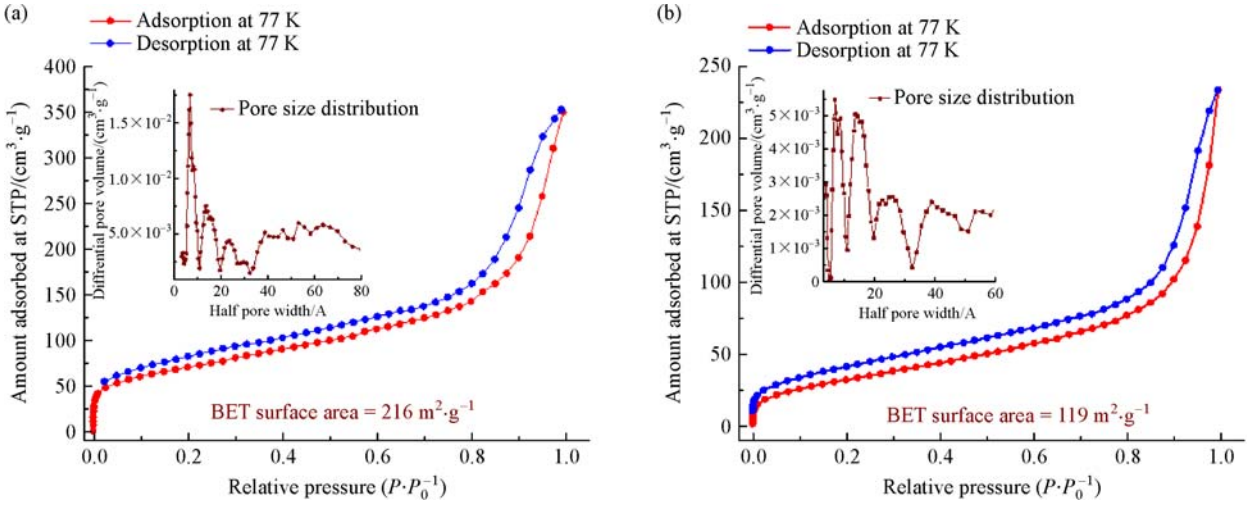

Fig. 7 N_2 adsorption-desorption isotherm of (a) **4** and (b) **5** measured at 77 K. Inset: corresponding pore size distribution curve

abilities to organic solvents. The solid state Ln(III) centered luminescence of **4** and **5** showed the variation in their emission properties when recording the spectra in presence of different organic solvents. The solid state Eu (III) emission recorded from a film made of **4** in presence of THF and CH_3CN was found to be quenched to 81% and 70% respectively, however, the emission was found to be increased to 148% in presence of MeOH, when compared to the emission of **4** in its dry state as shown in Fig. 8(a). The variation in the emission properties of **4** was further confirmed by measuring the changes in the excited state lifetimes (τ) of Eu(III). The 615 nm emission displayed a monoexponential decay curve indicating the single environment for the all three Eu(III) ions in **4**. The τ values obtained for Eu(III) emission from solid dry film of **4** was found to be 0.266 ms, and 0.297, 0.304 and 0.343 ms in presence of THF, CH_3CN and MeOH respectively as summarized in Table 1. Compound **5** also showed the variation in its Tb(III) centered emission in presence of organic solvents. Unlike **4**, **5** showed the quenching of emission in all the solvents tested. In presence of THF, CH_3CN and MeOH, the solid state Tb(III) centered emission from a film made of **5** was quenched to 30%, 65% and 47% respectively, when compared its emission in dry state as displayed in Fig. 8(b). The 545 nm band of Tb(III) emission from **5** was fit to monoexponential decay indicating the single environment of the all three Tb(III) ions. The τ values obtained for Tb(III) emission from solid dry film of **5** was found to be 0.543 ms, and 0.539, 0.498 and 0.597 ms in presence of THF, CH_3CN and MeOH respectively (Table 1).

Table 1 Summarized τ values for solid state Eu(III) and Tb(III) emission from **4** and **5** in dry state and in presence of organic solvents

	τ values for Eu(III) emission from **4**	τ values for Eu(III) emission from **5**
Solid film	0.266 ms	0.543 ms
THF	0.297 ms	0.539 ms
CH_3CN	0.304 ms	0.498 ms
MeOH	0.343 ms	0.597 ms

2.5 Probing the self-assembly formation of **4** and **5** in solution

The analysis of the self-assembly formation of **4** and **5** was also probed in aqueous solution at low concentration (~10^{-5} mol·L^{-1}) by observing the changes in the photophysical properties of **3**, and of the emerging self-assembly structures **4** and **5** by carrying out a series of photophysical titrations using UV-vis, fluorescence and lanthanide luminescence spectroscopy. Unlike the analysis of the solid material above (as bulk material), it was possible to probe the self-assembly formation between **1** and **2**, with the antenna **3**, at low concentration at pH 7.4 in 0.1 mol·L^{-1} Tris aqueous buffer. A stock solution (3 mL, 2.5 × 10^{-6} mol·L^{-1}) of **3** (as sodium salt form) was prepared and titrated against known volumes of a standard solution of either complex **4** or **5**. Following each addition, the UV-vis absorption and luminescence (fluorescence and phosphorescence) spectra were recorded after an equilibration time of 5 min. The formation of a ternary complex between **1** and **3** to yield **4** will be the main focus of the discussion that follows.

The self-assembly between **1** and **3** was first observed in solution by observing the changes in the UV-vis absorption spectra of **3**, upon addition of **1**, which, as it does not contain any antennae can be considered to be photophysically silent. The spectrum of the free ligand **3** was characterized by two main bands; a high energy one centered at *ca*. 207 nm, and a large two-pronged band with maxima at 296 and 314 nm, corresponding to the π-π* transitions of the phenyl rings (Fig. 9(a)). Sequential addition of **1** was later found to instigate a hypochromic shift in the latter band, with the concomitant formation of a new band at *ca*. 350 nm resulting in an isosbestic point at 322 nm. The binding isotherms are shown as insert in Fig. 9(a) for these changes, with the changes occurring

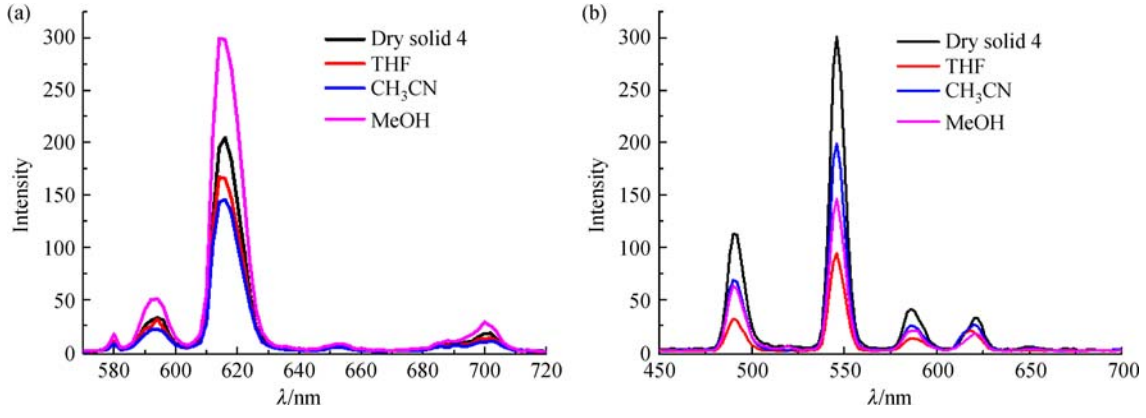

Fig. 8 Solid state emission spectrum of (a) **4** and (b) **5** recorded in dry state (black) and presence of THF (red), CH_3CN (blue) and MeOH (pink)

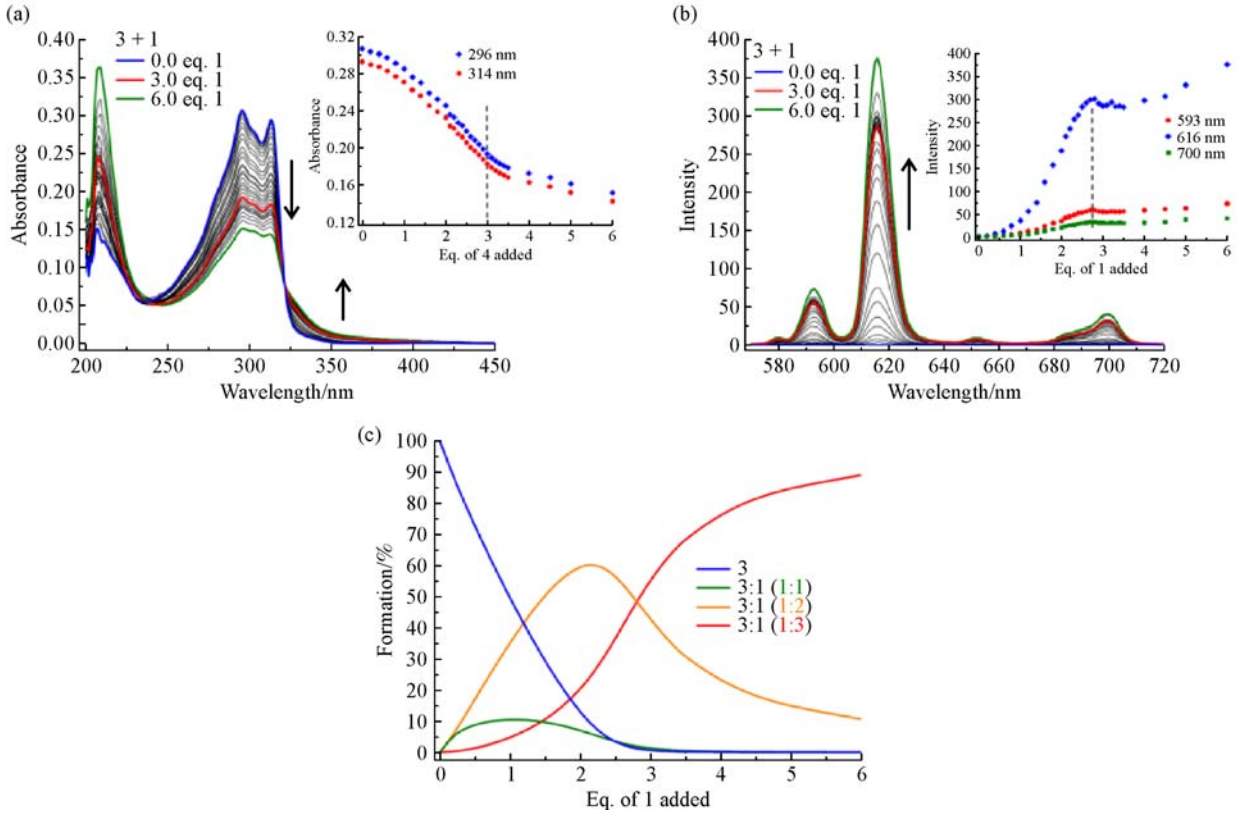

Fig. 9 (a) Changes in the absorption spectra of **3** (2.5×10^{-6} mol·L^{-1}) upon titrating with Eu(III) complex **1** (0.00 → 6.00 eq.) in 0.1 mol·L^{-1} Tris aqueous buffer (pH 7.4) at 298 K (Insert: Binding isotherms for the changes observed at 296 nm and 314 nm, respectively); (b) the evolution of the (phosphorescence) delayed Eu(III) emission of **4** with λ_{exc} = 296 nm demonstrating the formation of **4** *in situ* (Inset: Binding isotherms for the changes observed at 593 nm, 616 nm, and 700 nm); (c) the speciation-distribution diagram obtained from the fitting of the change in the absorption spectra (seen in Fig. 9(a)) using the nonlinear regression analysis program SPECFIT, demonstrating the stepwise formation of the 1:3 stoichiometry of **4** from **1** and **3**

steadily up till *ca*. 3 eq. of **1**, with these effects becoming less pronounced thereafter. The coordination of the benzoate groups of **3** to **1** was also evidenced upon excitation of 3 at 296 nm. Indeed, ligand excitation was found to yield phosphorescence spectra exhibiting the characteristic Eu(III)-centered emission structure, with bands centered at 580, 593, 616, 652 and 695 nm, respectively, as shown in Fig. 9(b), similar to those observed in the solid state for **4** (*c.f.* Fig. 2).

With no observable change in band fine-structure, all bands were seen to undergo an intensity increase with successive additions of **1**. This pattern of intensification was best visualized from the binding isotherms shown as inset in Fig. 9(b), where emission intensity was shown to rapidly rise before levelling off at *ca.* 3 eq. of **1**. Concomitantly, the broad fluorescence emission of **3**, centered at 371 nm, was also affected, being quenched upon the addition of **1**, indicating that the antenna was engaged in the population of the Eu(III) excited state; the quenching occurring within the same equivalent (of **1**) range as that seen for the emerging of the Eu(III) centered emission. This was also confirmed by monitoring the changes in the phosphorescence excitation spectra upon addition of 0 → 3 equivalents of **1** to a solution of **3**, the result demonstrating that the spectrum was structurally identical to the absorption spectrum of **1**, and the excitation spectra increased in intensity upon addition of **3**, as a consequence of the formation of a ternary complex between **1** and **3**, and enhanced population in the $^5D_0$ excited state of Eu(III).

The key intermediates and products of the self-assembly pathway at this low concentration of **1** and **3**, were elucidated by fitting the changes in the UV-vis absorption spectra and the Eu(III) emission spectra using nonliner regression analysis. From this analysis, the formation of three different species in solution were identified, namely, the formation of the 1:1, 1:2 and 1:3 stoichiometry for **3:1**, with associated binding constants as logβ = 19.74±0.18, 13.69±0.19 and 6.24±0.39, respectively. From these changes, and fitting, the speciation diagram shown in Fig. 9(c) was generated, demonstrating that at this low concentration, the self-assembly, being kinetically driven, results in the formation of the 1:3 stoichiometry in *ca*. 55% yield in solution upon addition of 3 equivalents of the Eu

(III) complex **1**, becoming the dominate species at higher equivalents of **1**, indicating the successful formation of the 1:3 complex **4** as depicted in Fig. 1. Furthermore, the constants representing the individual coordination steps were approximately additive, telling of independent binding at the three chelating sites with an absence of cooperativity (positive or negative).

The photophysical titration between **3** and **1** was repeated using D_2O as solvent. The changes observed in UV-vis absorption and Eu(III) centered phosphorescence spectra was analogous to the titrations performed in aqueous medium, and the Eu(III) excited state lifetimes of species was found to be slightly longer in case of D_2O (τ_{D_2O}) than observed in H_2O (τ_{H_2O}). This clearly indicated the removal of the Eu(III) centered luminescence quenching caused by OH groups in aqueous medium. The lifetimes of Eu(III) excited states recorded at an interval of 1.0 equivalent of metal ion addition in D_2O (τ_{D_2O}) and in H_2O (τ_{H2O}), and the q values (number of directly bound H_2O molecules to Eu(III)) for the corresponding species formed are summarized in Table 2. In all the species formed during course of titration, the q values were found to be 0.4 indicating no H_2O molecules was bound to Eu (III) and the successful complexation between **1** and **3**.

Strikingly, similar changes were seen in the UV-vis absorption titration between **3** and **2**, which yielded **5**, was found to that seen above for the formation of **4**. As previously observed, the distinctive two-pronged band (*ca*. 305 nm), characteristic of the free ligand, sustained a hypochromic shift with each addition of **2**, with a concomitant formation of a new band at *ca*. 350 nm within an isosbestic point at 322 nm, Fig. 10(a). The corresponding changes observed in the Tb(III) emission upon formation of **5** are shown in Fig. 10(b) for the evaluation of the 487, 545, 586, and 618 nm bands, representing the $^5D_4 \rightarrow {}^7F_J$ transitions (J = 6–3), respectively, confirming the formation of the desired self-assembly between **2** and **3** in solution. Again the fluorescence of **3** was found to decrease with increasing concentrations of **2**, the changes being most pronounced between $0 \rightarrow 3.5$ eq. of **2**, reflecting the formation of the desired 1:3 stoichiometry between **3** and **2**. Further analysis of the changes in the absorption spectra at 296 and 314 nm, using SPECFIT as above, showed the stepwise formation of the 1:3 stoichiometry; the speciation distribution being almost identical to that seen for the Eu (III) analog above (Fig. 10(c)); the 1:3 stoichiometry, being formed in *ca*. 60% yield at three equivalents of **2**, under these experimental conditions. At higher concentrations of **2**, the equilibrium process was further shifted to the formation of **5**, as can be seen in Fig. 10(c). These overall changes clearly demonstrate the formation of the 1:3 stoichiometry of **4** and **5** at the end-point of the titrations of **3** with both **1** and **2**, in solution at low concentration under kinetic control.

The photophysical titrations between **3** and **2** was repeated using D_2O as solvent, and the changes observed was identical to the observations made in case of aqueous medium. Similar to the observation made above, the Tb (III) excited state lifetimes of species was found to be slightly longer in of D_2O (τ_{D_2O}) than in H_2O (τ_{H_2O}) indicating the luminescence quenching by OH groups in aqueous medium. The of Tb(III) lifetimes recorded for titrations in D_2O (τ_{D_2O}) and in H_2O (τ_{H_2O}), and the q values for the corresponding species are summarized in Table 3. In all the species, the q values were found to be 0.4 indicating no H_2O molecules was bound to Tb(III) and the successful complexation between **2** and **3**.

3 Conclusions

Herein, we have demonstrated the formation of two self-assembly structures **4** and **5** formed from the use of the 1,3,5-benzene-trisethynylbenzoate ligand **3** with the Eu (III) and Tb(III) 1,4,7,10-tetraazacyclododecane complexes **1** and **2**. The self-assembly process was observed in solution by observing the changes in the absorption spectra of **3** and the emerging emission spectra of both **4** and **5** upon excitation of the antennae ligand **3**. Analysis of these changes demonstrated the stepwise formation of the 1:1, 1:2 and the 1:3 stoichiometry between **3** and either of these complexes, which emit with line-line emission bands characteristic for the fully coordinatively saturated complexes. The complexes were also formed using microwave assisted synthesis by using the 1:3 stoichiometry, and the resulting solids isolated were also characterized using various techniques; both (powder) samples being highly luminescent giving rise to characteristic red and green emission that was clearly visible to the naked eye for **4** and **5**, respectively. SEM images of the dropcasted solutions of these complexes revealed that the material obtained had a morphology that consisted of larger solid blocks having nano porous surface, while the ligand **3** consisted on fibrous branched network. Both **4** and **5**, were investigated for their ability to store gases such as CO_2 an N_2 and their solution properties were also investigated by observing the changes in the lanthanide centered emission in different

Table 2 Summary of τ_{H_2O} and τ_{D_2O} values of Eu(III) and the q values of the species during the titrations between **3** and **1** in H_2O and D_2O

Equiv. of Eu(III) added	1	2	3	4	5	6
H_2O	1.079	1.020	1.024	1.051	1.055	1.065
D_2O	1.297	1.231	1.218	1.245	1.266	1.285
q values	0.4	0.5	0.4	0.4	0.4	0.4

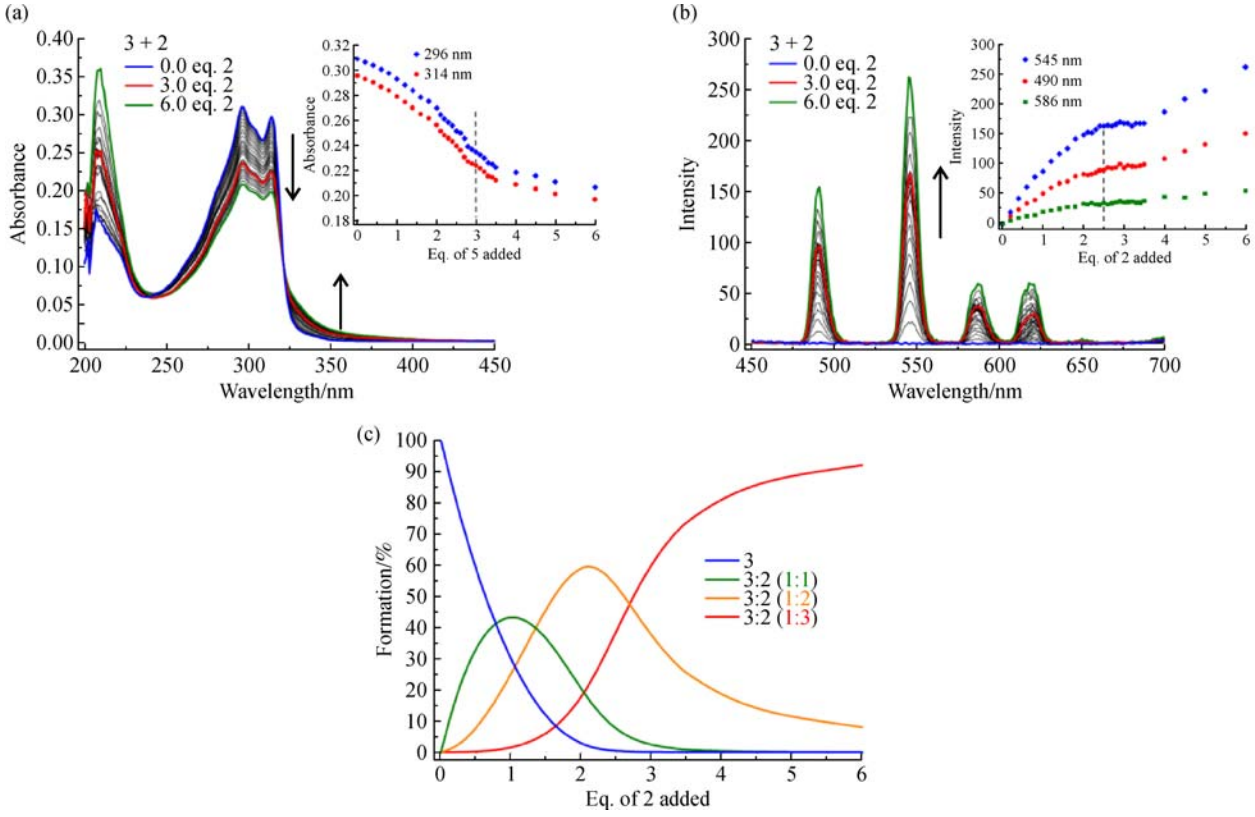

Fig. 10 (a) Changes in the absorption spectra of **3** (2.5×10^{-6} mol·L^{-1}) upon titrating with Eu(III) complex **2** (0.00 → 6.00 eq.) in 0.1 mol·L^{-1} Tris aqueous buffer (pH 7.4) at 298 K (Insert: Binding isotherms for the changes observed at 296 nm and 314 nm, respectively); (b) the evolution of the (phosphorescence) delayed Tb(III) emission of **5** with λ_{exc} = 296 nm demonstrating the formation of **4** *in situ* (Inset: Binding isotherms for the changes observed at 490, 545, and 586 nm); (c) the speciation-distribution diagram obtained from the fitting of the change in the absorption spectra (seen in Fig. 9(a)) using the nonlinear regression analysis program SPECFIT, demonstrating the stepwise formation of the 1:3 stoichiometry of **5** from **2** and **3**

Table 3 Summary of τ_{H_2O} and τ_{D_2O} values of Tb(III) and q values of the species during the titrations between **3** and **2** in H_2O and D_2O

Equiv. of Tb(III) added	1	2	3	4	5	6
τ_{H_2O}	1.079	1.020	1.024	1.051	1.055	1.065
τ_{D_2O}	1.297	1.231	1.218	1.245	1.266	1.285
q values	0.4	0.5	0.4	0.4	0.4	0.4

solvents. Overall, the result demonstrates that the 1:3 stochiometric self-assembly is unique; it leads to the formation of higher or hierarchically porours materials, most likely formed through electrostatic and π-π interactions, the properties of which can be probed using various techniques, including solid state luminescence. We are currently pursuing this area of research further, by developing other examples of cyclen based lanthanide complexes.

4 Experimental

General: all chemicals were purchased from Sigma-Aldrich Ireland Ltd., Acros Organics, TCI Ltd., and Chematech, and were used without further purification, unless otherwise stated. Melting Points were determined using an Electrothermal IA900 digital melting point apparatus. NMR spectra were recorded at 293 K using Bruker Spectrospin DPX-400 instrument, operating at 400.1 MHz for ^{1}H NMR and 100.6 MHz for ^{13}C NMR. Tetramethylsilane was used as an internal standard and chemical shifts were referenced relative to the internal non-deuterated solvent signal, with chemical shifts being expressed in parts per million (ppm or δ). For ^{1}H NMR spectra, the number of protons, splitting pattern, coupling constant where applicable, and proton assignment are also reported (in that order). Multiplicities are abbreviated as follows; singlet (s), doublet (d), triplet (t), quartet (q), quintet (qu), multiplet (m), and broad (br). High-resolution

mass spectrometry was performed using MALDI-Q-TOF-Premier instrument (Waters Corporation, Micromass MS technologies, Manchester, UK), using leucine enkephaline (H-Tyr-Gly-Gly-Phe-Leu-OH) as the standard reference (*m/z* = 556.2771); all accurate masses were reported within±5 ppm of the expected mass. Infrared spectra were recorded on a Perkin Elmer Spectrum One FT-IR spectrometer fitted with a universal ATR sampling accessory. TGA was performed on an analyzer equipped with an ultra-microbalance with a sensitivity of 0.1 mg. The temperature range was from 25°C to 800°C with a scan rate of 10°C·min^{-1} under N_2 purge.

General procedure for synthesis of **1** and **2**. Ligand 2,2',2''-(1,4,7,10-Tetraazacyclododecane-1,4,7-triyl)tris(*N*,*N*-dimethylacetamide) (0.028 g, 0.065 mmol, 1.00 eq.) and $Eu(CF_3SO_3)_3$ or $Tb(CF_3SO_3)_3$ (0.065 mmol, 1.00 eq.) were refluxed together, under an inert atmosphere, in freshly distilled CH_3CN (6 mL) for 24 h. Following reduction of the solvent volume to *ca*. 1 mL, the product was precipitated from swirling dry diethyl ether. Isolation by decanting afforded a yellow/brown solid the complex **1** (0.055 g, 0.054 mmol, 83% yield) or **2** (0.056 g, 0.054 mmol, 79% yield).

Complex **1**. m.p. decomposed above 180°C; HRMS (*m/z*) (MALDI$^+$) calculated for $C_{21}H_{40}N_7O_6SF_3Eu$ *m/z* = 728.1925 $[M - 2CF_3SO_3 - H]^+$. Found *m/z* = 728.1909; ^{1}H NMR (400 MHz, CD_3CN-d_3) δ_H: 27.76, 18.39, 15.55, 11.47, 5.49, 3.37, 2.74, −1.49, −3.54, −6.25, −10.19, −12.30, −13.94; IR υ_{max} (cm^{-1}): 3434, 2982, 2927, 2884, 1625, 1508, 1459, 1438, 1413, 1280, 1258, 1173, 1084, 1031, 960, 824, 762, 641, 573, 518.

Complex **2**. m.p. decomposed above 190°C; HRMS (*m/z*) (MALDI$^+$) calculated for $C_{21}H_{40}N_7O_6SF_3Tb$ *m/z* = 734.1966 $[M - 2CF_3SO_3 - H]^+$. Found *m/z* = 734.1940; ^{1}H NMR (400 MHz, CD_3CN-d_3) δ_H: 183.78, 142.59, 117.67, 93.7, 75.9, 42.97, 25.3, 17.96, 17.38, 15.44, 14.98, 13.10, 12.39, 11.29, 8.76, 7.25, −36.6, −58.37, −70.86, −105.92, −141.03; IR υ_{max} (cm^{-1}): 3434, 2957, 2927, 2856, 1625, 1508, 1465, 1438, 1412, 1279, 1256, 1171, 1084, 1030, 960, 824, 761, 640, 574, 518.

General procedure for synthesis of **4** and **5**. Compounds **4** and **5** were prepared by reacting the relevant complex **1** or **2** (3.6 equiv.) with **3** (1 equiv.) in CH_3CN (5 mL) under microwave radiation at 70°C for 1 h. The reaction mixture was subsequently cooled to room temperature and the resulting white solid was collected by decanting the liquid and dried under vacuum to obtain **4** or **5** as light brown solids.

Complex 4. m.p. decomposed above 221°C; IR υ_{max} (cm^{-1}): 3335.9, 2979.4, 2887.4, 1605.1, 1576.4, 1524.6, 1403.9, 1283.1, 1179.6, 1099.1, 863.4, 782.9, 748.4, 696.6.

Complex 5. m.p. decomposed above 227°C; IR υ_{max} (cm^{-1}): 3358.9, 2979.6, 2886, 1681.5, 1605.5, 1576.2, 1523.6, 1389.1, 1254.6, 1786.6, 1102.6, 956.4, 862.8, 786.8, 699.1.

UV-vis absorption and luminescence spectroscopy. Using a 1.0 cm path length quartz cell, UV-vis absorption and luminescence spectra were recorded using a Varian CARY 50 and a Varian Cary Eclipse spectrophotometer, respectively. All measurements were performed at 298 K using spectrophotometric grade solvents. Emission (fluorescence, phosphorescence and excitation) spectra and lifetimes were recorded on a Varian Cary Eclipse Fluorimeter. The concentrations of the ligand **3** and complexes (**1** or **2**) analyzed were the same for both UV-vis and luminescence titrations. Baseline correction measurements were employed for all UV-vis spectra, where the blank was a sample of the solvent system in which the titration was performed. The parameters used for the UV-vis absorption and luminescence titration studies are listed below. Voltage was adjusted as necessary to prevent signal saturation.

UV-vis absorption settings for titrations. Baseline correction was applied for all UV-vis absorption spectra. The absorption data was collected between 200 and 450 nm using a scan rate of 600 min^{-1}. Excitation slit, and emission slit used were 1 nm each.

Phosphorescence settings for titrations. The luminescence data was collected between 570 and 720 nm for the Eu(III) emission and 450 and 650 nm for the Tb(III) using the excitation wavelength of 296 nm. Excitation slit, and emission slit used were 20 nm and 1.5 nm, with flash count of 1. A delay time of 0.1 ms, Gate time of 5 ms, and total decay time of 0.02 s were used to record the time delayed emission spectrum. An averaging time of 0.1 s were applied, and the data were recorded at an interval of 1 nm resolution.

Luminescence settings for the lifetime measurements. The Phosphorescence lifetimes of the Eu($^5D_0$) and Tb($^5D_4$) excited states for the synthesized complexes and self-assembles **4** and **5**, respectively, were conducted using a Varian Carey Eclipse Fluorimeter in time-resolved mode at 298 K. All lifetime values were obtained from an average of 3 independent measurements, and each measurement was recorded with a different gate time in the range 0.02–0.03 ms. Excitation wavelength of 281 nm was used, and the resulting emission intensitis at 616 and 545 nm which corresponds to the maxima of the Eu(III) $^5D_0 \rightarrow {}^7F_2$ Tb (III) and $^5D_4 \rightarrow {}^7F_5$ transitions, respectively were monitored as a functions of total decay time of 20 ms.

Solid state emission and sensing properties of **4** and **5**. solids **4** and **5** was sonicated (10 min) in H_2O, and the resulting fine suspension was dropcasted in quartz plates and dried in air (12 h) and vacuum (12 h) to obtain a thin solid film of **4** and **5**. This film of **4** and **5** was used to measure the solid state emission and lifetime of Eu(III) and Tb(III) in dry state and in presence of organic solvents for their sensing properties.

Morphology studies of the ligand **3** and Ln-self-assemblies **4** and **5**. The morphology of **4** and **5** was imaged by Field emission scanning electron microscopy

(FE-SEM) with an SE2 or an inlens detector. The sample was prepared by drop-casting the solution or suspension of the as-synthesized **3**, **4** and **5** (1% $wt \cdot v^{-1}$ in Millipore water) on silica wafers and dried in air (12 h) and under vacuum (2–3 h). All samples were coated with Au before the imaging.

Gas uptake studies. Gas sorption isotherms were measured using a Quantachrome Autosorb IQ gas sorption analyzer. Chemically pure (CP) grade He, N_2, H_2, and CO_2 gases from BOC gases were used for measurements. The as-synthesized complexes **4** and **5** were immersed in diethyl ether for 3 d and was refreshed 3 times with fresh diethyl ether. The resulting solvent exchanged solids was transferred to a quartz cell. The sample was evacuated under vacuum at 30°C for 3 h and then slowly heated to 100°C over 10 h and held at 100°C for a further 5 h. The isotherms at 77 K were measured in a water-ice-acetone bath. The surface area was calculated by the BET method. Pore size distribution was calculated using a commercial kernel equilibrium model of N_2 at 77 K on carbon, slit pore NLDFT (included in Quantachrome ASiQwin version 2.02 software package). This model is applicable to pore width ranges of 0.35 to 40 nm. The 2015 IUPAC technical report [66] recommends the use of NLDFT based methods for pore size analysis of nanoporous materials.

Acknowledgements The authors gratefully acknowledge Science Foundation Ireland (PI awards 13/IA/1865 to T.G. and 13/IA/1896 to W.S.), the Irish Research Council (Postgraduate Scholarship to DC), the European Research Council (CoG 2014 – 647719 to W.S.) and the School of Chemistry, Trinity College Dublin.

References

1. Sun M, Chen C, Chen L, Su B. Hierarchically porous materials: Synthesis strategies and emerging applications. Frontiers of Chemical Science and Engineering, 2016, 10(3): 301–347
2. Savyasachi A J, Kotova O, Shanmugaraju S, Bradberry S J, Ó'Máille G M, Gunnlaugsson T, Ó'Máille G M, Gunnlaugsson T. Supramolecular chemistry: A toolkit for soft functional materials and organic particles. Chem, 2017, 3(5): 764–811
3. Zhang Z, Zaworotko M J. Template-directed synthesis of metal-organic materials. Chemical Society Reviews, 2014, 43(16): 5444–5455
4. Kreno L E, Leong K, Farha O K, Allendorf M, Van Duyne R P, Hupp J T. Metal-organic framework materials as chemical sensors. Chemical Reviews, 2012, 112(2): 1105–1125
5. Barry D E, Caffrey D F, Gunnlaugsson T. Lanthanide-directed synthesis of luminescent self-assembly supramolecular structures and mechanically bonded systems from acyclic coordinating organic ligands. Chemical Society Reviews, 2016, 45(11): 3244–3274
6. Bünzli J C G. Lanthanide luminescence for biomedical analyses and imaging. Chemical Reviews, 2010, 110(5): 2729–2755
7. Thibon A, Pierre V C. Principles of responsive lanthanide-based luminescent probes for cellular imaging. Analytical and Bioanalytical Chemistry, 2009, 394(1): 107–120
8. Bradberry S J, Savyasachi A J, Martinez-Calvo M, Gunnlaugsson T. Development of responsive visibly and NIR luminescent and supramolecular coordination self-assemblies using lanthanide ion directed synthesis. Coordination Chemistry Reviews, 2014, 273–274: 226–241
9. Lincheneau C, Stomeo F, Comby S, Gunnlaugsson T. Recent highlights in the use of lanthanide-directed synthesis of novel supramolecular (luminescent) self-assembly structures such as coordination bundles, helicates and sensors. Australian Journal of Chemistry, 2011, 64(10): 1315–1326
10. Dunning S G, Nuñez A J, Moore M D, Steiner A, Lynch V M, Sessler J L, Holliday B J, Humphrey S M. A sensor for trace H_2O detection in D_2O. Chem, 2017, 2(4): 579–589
11. Hawes C S, Gunnlaugsson T. Multichannel luminescent lanthanide polymers as ratiometric sensors for D_2O. Chem, 2017, 2(4): 463–465
12. Tobin G, Comby S, Zhu N, Clérac R, Gunnlaugsson T, Schmitt W. Towards multifunctional lanthanide-based metal-organic frameworks. Chemical Communications, 2015, 51(68): 13313–13316
13. Kotova O, Daly R, dos Santos C M G, Boese M, Kruger P E, Boland J J, Gunnlaugsson T. Europium-directed self-assembly of a luminescent supramolecular gel from a tripodal terpyridine-based ligand. Angewandte Chemie International Edition, 2012, 51(29): 7208–7212
14. Daly R, Kotova O, Boese M, Gunnlaugsson T, Boland J J. Chemical nano-gardens: Growth of salt nanowires from supramolecular self-assembly gels. ACS Nano, 2013, 7(6): 4838–4845
15. Martínez-Calvo M, Kotova O, Möbius M E, Bell A P, McCabe T, Boland J J, Gunnlaugsson T. Healable luminescent self-assembly supramolecular metallogels possessing lanthanide (Eu/Tb) dependent rheological and morphological properties. Journal of the American Chemical Society, 2015, 137(5): 1983–1992
16. Kotova O, Comby S, Lincheneau C, Gunnlaugsson T. White-light emission from discrete heterometallic lanthanide-directed self-assembled complexes in solution. Chemical Science, 2017, 8(5): 3419–3426
17. Montgomery C P, Murray B S, New E J, Pal R, Parker D. Cell-penetrating metal complex optical probes: Targeted and responsive systems based on lanthanide luminescence. Accounts of Chemical Research, 2009, 42(7): 925–937
18. Kitchen J A. Lanthanide-based self-assemblies of 2,6-pyridyldicarboxamide ligands: Recent advances and applications as next-generation luminescent and magnetic materials. Coordination Chemistry Reviews, 2017, 340: 232–246
19. Byrne J P, Kitchen J A, O'Brien J E, Peacock R D, Gunnlaugsson T. Lanthanide directed self-assembly of highly luminescent supramolecular "peptide" bundles from α-amino acid functionalized 2,6-bis(1,2,3-triazol-4-yl)pyridine (btp) ligands. Inorganic Chemistry, 2015, 54(4): 1426–1439
20. Byrne J P, Kitchen J A, Gunnlaugsson T. The btp [2,6-bis(1,2,3-triazol-4-yl)pyridine] binding motif: A new versatile terdentate ligand for supramolecular and coordination chemistry. Chemical Society Reviews, 2014, 43(15): 5302–5325
21. Zhang C, Shen X, Sakai R, Gottschaldt M, Schubert U S, Hirohara S, Tanihara M, Yano S, Obata M, Xiao N, et al. Syntheses of 3-arm and 4-arm star-branched polystyrene Ru(II) complexes by the click-

to-chelate approach. Journal of Polymer Science. Part A: Polymer Chemistry, 2011, 49(3): 746–753
22. Munuera L, O'Reilly R K. Using metal-ligand interactions for the synthesis of metallostar polymers. Dalton Transactions, 2010, 39(2): 388–391
23. Xiao N, Chen Y, Shen X, Zhang C, Yano S, Gottschaldt M, Schubert U S, Kakuchi T, Satoh T. Synthesis of miktoarm star copolymer Ru(II) complexes by click-to-chelate approach. Polymer Journal, 2012, 45(2): 216–225
24. Meudtner R M, Stefan H. Responsive backbones based on alternating triazole-pyridine/benzene copolymers: From helically folding polymers to metallosupramolecularly crosslinked gels. Macromolecular Rapid Communications, 2008, 29(4): 347–351
25. Meudtner R M, Hecht S. Helicity inversion in responsive foldamers induced by achiral halide ion guests. Angewandte Chemie International Edition, 2008, 47(26): 4926–4930
26. McCarney E P, Byrne J P, Twamley B, Martínez-Calvo M, Ryan G, Möbius M E, Gunnlaugsson T. Self-assembly formation of a healable lanthanide luminescent supramolecular metallogel from 2,6-bis(1,2,3-triazol-4-yl)pyridine (btp) ligands. Chemical Communications, 2015, 51(74): 14123–14126
27. Byrne J P, Kitchen J A, Kotova O, Leigh V, Bell A P, Boland J J, Albrecht M, Gunnlaugsson T. Synthesis, structural, photophysical and electrochemical studies of various d-metal complexes of btp [2,6-bis(1,2,3-triazol-4-yl)pyridine] ligands that give rise to the formation of metallo-supramolecular gels. Dalton Transactions, 2014, 43(1): 196–209
28. Crowley J D, Bandeen P H. A multicomponent CuAAC "click" approach to a library of hybrid polydentate 2-pyridyl-1,2,3-triazole ligands: New building blocks for the generation of metallosupramolecular architectures. Dalton Transactions, 2010, 39(2): 612–623
29. Byrne J P, Blasco S, Aletti A B, Hessman G, Gunnlaugsson T. Formation of self-templated 2,6-bis(1,2,3-triazol-4-yl)pyridine [2] catenanes by triazolyl hydrogen bonding: Selective anion hosts for phosphate. Angewandte Chemie International Edition, 2016, 55 (31): 8938–8943
30. Byrne J P, Martínez-Calvo M, Peacock R D, Gunnlaugsson T. Chiroptical probing of lanthanide-directed self-assembly formation using btp ligands formed in one-pot diazo-transfer/deprotection click reaction from chiral amines. Chemistry, 2016, 22(2): 486–490
31. Heffern M C, Matosziuk L M, Meade T J. Lanthanide probes for bioresponsive imaging. Chemical Reviews, 2014, 114(8): 4496–4539
32. Pal R, Parker D. A ratiometric optical imaging probe for intracellular pH based on modulation of europium emission. Organic & Biomolecular Chemistry, 2008, 6(6): 1020–1033
33. Pal R, Parker D. A single component ratiometric pH probe with long wavelength excitation of europium emission. Chemical Communications, 2007, (5): 474–476
34. dos Santos C M G, Harte A J, Quinn S J, Gunnlaugsson T. Recent developments in the field of supramolecular lanthanide luminescent sensors and self-assemblies. Coordination Chemistry Reviews, 2008, 252(23–24): 2512–2527
35. Sénéchal-David K, Leonard J P, Plush S E, Gunnlaugsson T. Supramolecular self-assembly of mixed f-d metal ion conjugates. Organic Letters, 2006, 8(13): 2727–2730
36. Gunnlaugsson T. Luminescent europium tetraazamacrocyclic complexes with wide range pH sensitivity. Chemical Communications, 1998, (4): 511–512
37. Truman L K, Bradberry S J, Steve C, Oxana K, Thorfinnur G. Luminescent europium tetraazamacrocyclic complexes with wide range pH sensitivity. ChemPhysChem, 2017, 18(13): 1746–1751
38. Bradberry S J, Byrne J P, McCoy C P, Gunnlaugsson T. Lanthanide luminescent logic gate mimics in soft matter: [H^+] and [F^-] dual-input device in a polymer gel with potential for selective component release. Chemical Communications, 2015, 51(92): 16565–16568
39. Surender E M, Bradberry S J, Bright S A, McCoy C P, Williams D C, Gunnlaugsson T. Luminescent lanthanide cyclen-based enzymatic assay capable of diagnosing the onset of catheter-associated urinary tract infections both in solution and within polymeric hydrogels. Journal of the American Chemical Society, 2017, 139(1): 381–388
40. dos Santos C M G, Fernández P B, Plush S E, Leonard J P, Gunnlaugsson T. Lanthanide luminescent anion sensing: evidence of multiple anion recognition through hydrogen bonding and metal ion coordination. Chemical Communications, 2007, (32): 3389–3391
41. Caffrey D F, Gunnlaugsson T. Displacement assay detection by a dimeric lanthanide luminescent ternary Tb(III)-cyclen complex: High selectivity for phosphate and nitrate anions. Dalton Transactions, 2014, 43(48): 17964–17970
42. Aletti A B, Gillen D M, Gunnlaugsson T. Luminescent/colorimetric probes and (chemo-) sensors for detecting anions based on transition and lanthanide ion receptor/binding complexes. Coordination Chemistry Reviews, 2018, 354: 98–120
43. Plush S E, Gunnlaugsson T. Solution studies of trimetallic lanthanide luminescent anion sensors: Towards ratiometric sensing using an internal reference channel. Dalton Transactions, 2008, (29): 3801–3804
44. Comby S, Surender E M, Kotova O, Truman L K, Molloy J K, Gunnlaugsson T. Lanthanide-functionalized nanoparticles as MRI and luminescent probes for sensing and/or imaging applications. Inorganic Chemistry, 2014, 53(4): 1867–1879
45. Kotova O, Comby S, Gunnlaugsson T. Sensing of biologically relevant d-metal ions using a Eu(III)-cyclen based luminescent displacement assay in aqueous pH 7.4 buffered solution. Chemical Communications, 2011, 47(24): 6810–6812
46. McMahon B, Mauer P, McCoy C P, Lee T C, Gunnlaugsson T. Selective imaging of damaged bone structure (microcracks) using a targeting supramolecular Eu(III) complex as a lanthanide luminescent contrast agent. Journal of the American Chemical Society, 2009, 131(48): 17542–17543
47. Comby S, Tuck S A, Truman L K, Kotova O, Gunnlaugsson T. New trick for an old ligand! The sensing of Zn(II) using a lanthanide based ternary Yb(III)-cyclen-8-hydroxyquinoline system as a dual emissive probe for displacement assay. Inorganic Chemistry, 2012, 51(19): 10158–10168
48. Truman L K, Comby S, Gunnlaugsson T. pH-responsive luminescent lanthanide-functionalized gold nanoparticles with "on-off" ytterbium switchable near-infrared emission. Angewandte Chemie International Edition, 2012, 51(38): 9624–9627

49. Boulay A, Deraeve C, Vander Elst L, Leygue N, Maury O, Laurent S, Muller R N, Mestre-Voegtlé B, Picard C. Terpyridine-based heteroditopic ligand for $Ru^{II}Ln_3^{III}$ metallostar architectures (Ln = Gd, Eu, Nd, Yb) with MRI/optical or dual-optical responses. Inorganic Chemistry, 2015, 54(4): 1414–1425
50. Nonat A M, Allain C, Faulkner S, Gunnlaugsson T. Mixed d-f_3 coordination complexes possessing improved near-infrared (NIR) lanthanide luminescent properties in aqueous solution. Inorganic Chemistry, 2010, 49(18): 8449–8456
51. Sénéchal-David K, Pope S J A, Quinn S, Faulkner S, Gunnlaugsson T. Sensitized near-infrared lanthanide luminescence from Nd(III)- and Yb(III)-based cyclen-ruthenium coordination conjugates. Inorganic Chemistry, 2006, 45(25): 10040–10042
52. Debroye E, Parac-Vogt T N. Towards polymetallic lanthanide complexes as dual contrast agents for magnetic resonance and optical imaging. Chemical Society Reviews, 2014, 43(23): 8178–8192
53. Dehaen G, Eliseeva S V, Verwilst P, Laurent S, Vander Elst L, Muller R N, De Borggraeve W, Binnemans K, Parac-Vogt T N. Tetranuclear d-f metallostars: Synthesis, relaxometric, and luminescent properties. Inorganic Chemistry, 2012, 51(16): 8775–8783
54. Dehaen G, Eliseeva S V, Kimpe K, Laurent S, Vander Elst L, Muller R N, Dehaen W, Binnemans K, Parac-Vogt T N. A self-assembled complex with a titanium(IV) catecholate core as a potential bimodal contrast agent. Chemistry, 2012, 18(1): 293–302
55. Verwilst P, Eliseeva S V, Vander Elst L, Burtea C, Laurent S, Petoud S, Muller R N, Parac-Vogt T N, De Borggraeve W M. A tripodal ruthenium-gadolinium metallostar as a potential $\alpha_v\beta_3$ integrin specific bimodal imaging contrast agent. Inorganic Chemistry, 2012, 51(11): 6405–6411
56. Gunnlaugsson T, Harte A J, Leonard J P, Nieuwenhuyzen M. Delayed lanthanide luminescence sensing of aromatic carboxylates using heptadentate triamide Tb(III) cyclen complexes: The recognition of salicylic acid in water. Chemical Communications, 2002, (18): 2134–2135
57. Castellano R K, Rebek J. Formation of discrete, functional assemblies and informational polymers through the hydrogen-bonding preferences of calixarene aryl and sulfonyl tetraureas. Journal of the American Chemical Society, 1998, 120(15): 3657–3663
58. Zhu N, Tobin G, Schmitt W. Extending the family of Zn-based MOFs: Synthetic approaches to chiral framework structures and MOFs with large pores and channels. Chemical Communications, 2012, 48(30): 3638–3640
59. Zhu N, Lennox M J, Düren T, Schmitt W. Polymorphism of metal-organic frameworks: Direct comparison of structures and theoretical N_2-uptake of topological pto- and tbo-isomers. Chemical Communications, 2014, 50(32): 4207–4210
60. Zhu N, Sensharma D, Wix P, Lennox M J, Duren T, Wong W Y, Schmitt W. Framework isomerism: Highly augmented copper(II)-paddlewheel-based mof with unusual (3,4)-net topology. European Journal of Inorganic Chemistry, 2016, 2016(13–14): 1939–1943
61. Zhu N, Lennox M J, Tobin G, Goodman L, Düren T, Schmitt W. Hetero-epitaxial approach by using labile coordination sites to prepare catenated metal-organic frameworks with high surface areas. Chemistry, 2014, 20(13): 3595–3599
62. Furukawa H, Ko N, Go Y B, Aratani N, Choi S B, Choi E, Yazaydin A Ö, Snurr R Q, O'Keeffe M, Kim J, Yaghi O M. Ultrahigh porosity in metal-organic frameworks. Science, 2010, 329(5990): 424–428
63. Byrne K, Zubair M, Zhu N, Zhou X P, Fox D S, Zhang H, Twamley B, Lennox M J, Düren T, Schmitt W. Ultra-large supramolecular coordination cages composed of endohedral Archimedean and Platonic bodies. Nature Communications, 2017, 8(8): 15268
64. Yao Q, Bermejo Gómez A, Su J, Pascanu V, Yun Y, Zheng H, Chen H, Liu L, Abdelhamid H N, Martín-Matute B, Zou X. Series of highly stable isoreticular lanthanide metal–organic frameworks with expanding pore size and tunable luminescent properties. Chemistry of Materials, 2015, 27(15): 5332–5339
65. Suh M P, Choi H J, So S M, Kim B M. A new metal-organic open framework consisting of threefold parallel interwoven (6,3) nets. Inorganic Chemistry, 2003, 42(3): 676–678
66. Thommes M, Kaneko K, Neimark A V, Olivier J P, Rodriguez-Reinoso F, Rouqerol J, Sing K S W. Physisortion of gases, with special reference to the evaluation of surface area and pore size distribution (IUPAC Technical Report). Pure and Applied Chemisty, 2015, 87(9–10): 1051–1069